



Original article

Energy input adaptation according to part geometry in selective laser melting through empirical modelling of thermal emission

Emra Vasilevska^a, Ali Gökhan Demir^b, Bianca Maria Colosimob^b,
*Valentina Gečevska^a, Barbara Previtali^b

^aSs. Cyril and Methodius University in Skopje, Faculty of Mechanical Engineering - Skopje, Ruger Bosković 18,
1000 Skopje, North Macedonia

^bPolitecnico di Milano, Department of Mechanical Engineering, Via La Masa 1, 20156 Milan, Italy

ABSTRACT

Common practice in Selective Laser Melting (SLM) is employing a series of fixed process parameters throughout the whole build. However, process thermal conditions strongly depend on the local geometry of the part. Formation of some common defects, including swelling regions and elevated zones, emerges in critical corner areas due to excessive heat accumulation when constant parameters are used. Adaptation of energy input according to the geometry of the processed zone is highly desirable for avoiding defect formation. To assess the processing conditions, observation of the melt pool and its variation as a function of the process parameters with a coaxial camera operating in near infrared (NIR) demonstrated to be a feasible option. This work develops an empirical model that gives the correct amount of energy input to achieve stable melt pool depending on the single vector length, hence the part geometry. The model was validated on a prototype SLM system, and the results showed that controlling the process parameters considerably improves the geometrical accuracy of the parts with sharp edges prone to hot spot formation.

Key words: Additive manufacturing, Geometrical accuracy, Melt pool monitoring, Process modelling, Energy input control;

1. INTRODUCTION

Selective Laser Melting (SLM) is getting broad recognition amongst the metal additive manufacturing processes due to the possibility to produce complex geometries with internal channels and lightweight structures, otherwise impossible with conventional manufacturing methods. However, the lack of process repeatability and product quality diminishes its wide acceptance in highly regulated industries [1]. One of the main factors accountable for the defect occurrence is the inaccurate choice of process parameters [2]. The scanning parameters are commonly set experimentally, calibrated to achieve high density in bulk geometries, and are subsequently employed to produce the whole part. However, a fixed set of parameters do not account for the geometrical variations between and within parts. The parameters which result with nominal part

density in stable regions, may generate defects when scanning critical regions such as overhangs or acute corners where overheating occurs and leads to geometrical and microstructural defects [3,4]. Common geometrical defect occurring in regions with peaked ends due to heat accumulation and buildup of residual thermal stress is the swelling defect, which is the topic investigated in this study. The swelling is defined as elevated ridges of solidified material which warp or curl upwards out of the powder layer [5].

Simulations of the melting and solidification behavior of the SLM process with Finite Element Analysis (FEA) have shown its possibility to optimize the process parameters for theoretically achieving certain part density [6]. Nevertheless, effective simulation tools able to adapt process parameters depending on the part geometry are still to be developed.

* Corresponding author's e-mail: valentina.gecevska@mf.edu.mk

Published by the University of Novi Sad, Faculty of Technical Sciences, Novi Sad, Serbia.
This is an open access article distributed under the CC BY-NC-ND 4.0 terms and conditions

To have an insight into the momentary conditions of the process, several works developed different types of off-axial and coaxial monitoring setups [7]. The thermal conditions and hence the exhibited melt pool during the process is correlated to the final product quality [8].

Real-time monitoring of the melt pool dimensions during the scanning process is feasible with coaxial monitoring setup with camera, which provides high spatial resolution of the observed region. Commercial solutions for coaxial monitoring of the melt pool have also been produced. While these solutions are more widely adapted as a means for quality control during and after the build process [7], their use for process parameter development has not received much attention.

Hence, the present work develops a process model for adapting the laser energy input by modulating the laser power as a function of the part geometry, for generating stable melting conditions and avoiding the swelling defect in critical sharp regions of the part. For the development of the empirical model a coaxial melt pool monitoring system was employed. According to Fox et al. [9], controlling the melt pool dimensions throughout the process can ensure robust part quality. Therefore, the area of the melt pool was selected as a monitoring feature which demonstrates the process conditions. Demir et al. [10] proved that employing a different set of process parameters in bulk region and in thin structure results in stable melt pool in the whole part geometry.

The developed empirical model in the presented work optimizes the parameters as a function of the length of the scan vectors, hence the part geometry.

2. CONTROL OF LASER ENERGY DENSITY BY POWER MODULATION

During SLM, within a given layer several scan vectors are generated, which are then melted with a chosen energy input. The given energy input is required to melt a specific mass of material. To find the laser energy density delivered at each point of the process, the following equation is used:

$$E[J/mm^3] = \frac{P}{h \cdot z \cdot v} \quad (1)$$

where h [μm] is the hatch distance, z [μm] is the layer thickness, P [W] is the input power and v [mm/s] is the scan speed of the laser beam.

The laser can be operated in two modes: continuous wave (CW) and pulsed wave (PW) [11]. When scanning in CW mode, the laser source outputs a continuous power profile that interacts with the material at all times. The laser is scanned with a constant speed and constant power equal to P_{cw} . In PW mode, the laser intermittently interacts with the powder, meaning that the laser beam is not continuously brought to the material, but only at the instances when there is an active pulse [12]. As a result, the laser power will no longer remain constant with respect to time, but it will be modulated. The scanning speed in PW mode is constant, which implies that the laser beam moves continuously while the laser is emitting and not emitting. The resulting

average power of the pulsed beam travelling with constant velocity is calculated as:

$$P_{avg,PW}[W] = P_{peak,PW} \cdot \delta \quad (2)$$

where $P_{peak,PW}$ [W] is the peak laser power of the impulse, and δ [-] is the duty cycle. The duty cycle δ expresses the laser on-time over the whole pulsation period:

$$\delta = \frac{t_{on}}{t_{on}+t_{off}} = \frac{t_{on}}{t_{tot}} \quad (3)$$

where t_{on} [s] is the period of time when the laser is emitting during one pulse, and t_{off} [s] is the period of time the laser is not emitting during one pulse. Therefore, as δ increases, the laser moves from PW to CW scanning mode, until reaching value equal to 1 which corresponds to laser scanning in CW mode. The modulation frequency f describes the temporal behavior of the pulse emission, and is defined as:

$$f[Hz] = \frac{1}{t_{tot}} \quad (4)$$

3. EXPERIMENTAL HARDWARE AND SOFTWARE

3.1. Open SLM platform

An open and custom-made SLM platform ‘‘Penelope’’ was used to conduct the experimental work [13]. The powder bed is placed in a closed chamber where an inert argon atmosphere is created. The laser source employed in the experiment is a single mode fiber laser (IPG Photonics YLR-150/750-QCW-AC, Cambridge, MA, USA) which can emit in both CW and PW regime by power modulation. The laser optical chain consists of a collimating unit with a focal length of 50 mm, a focus shifting two-lens system (VarioScan 20, Scanlab, Puchheim, Germany), and a 420 mm f-theta lens, while the deflection of the laser beam toward the building platform is achieved using two galvanometric mirrors.

The main specifications of the open SLM platform and its optical chain can be found in Table 1.

Table 1 Main characteristics of the open SLM system

Parameter	Value
Laser emission wavelength, λ	1070 nm
Max. laser power, P_{peak}	250 W
Max. laser modulation frequency	10 kHz
Beam quality factor, M^2	1.1
Nominal beam diameter at the focal plane, d_0 ($1/e^2$)	70 μm
Working volume	60×60×20 mm ³

3.2. Material

In the experimental work, gas-atomized stainless steel AISI 316L (Cogne Acciai, Brescia, Italy) powder was used, with a packing density of 4.07 g/cm³, and powder size distribution measured as D10: 22.9 μm , D50: 31.9 μm ; and D90: 44.3 μm .

3.3. Coaxial monitoring module

To acquire the thermal emission of the melt pool, a coaxial monitoring system was designed and connected directly onto the machine working head, thus looking through the scan head to observe the zone of interaction of laser beam and powder bed. A scheme of the optical chain is presented in Fig. 1. The NIR range was viewed with an industrial CMOS camera (Ximea xiQ USB Vision, Münster, Germany) and two optical filters positioned before the camera which limit the acquisition wavelength between 850 and 1000 nm (FEL0850 and FESH1000, Thorlabs, Newton, NJ, USA). A focusing lens (Camera Adapter, Scanlab GmbH, Puchheim, Germany) was used to fix the image plane with a focal length of 120 mm. The employed 8-bit camera sensor has a size of 1280×1204 pixel², and pixel size of 4.8×4.8 μm². The camera field of view was calibrated to 4.3×4.3 mm² by adapting the region of interest, in order to view the full length of the melt pool in all directions, achieving a spatial resolution of 14 μm/pixel and an acquisition rate of 1200 fps with an exposure time of 29 μs. As schematically demonstrated in Fig. 1, the process emission travels through the f-theta lens, galvanometric mirrors, and dichroic mirror reflective between 400 and 1000 nm, towards the camera sensor.

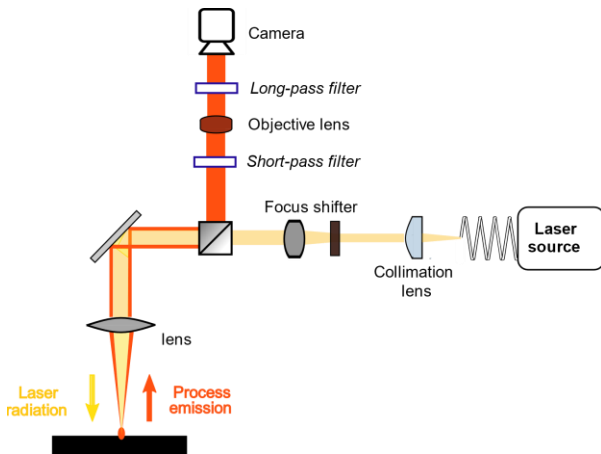


Fig. 1 Optical chain of the coaxial monitoring setup

3.4. Extraction and measurement of melt pool area

The acquired NIR images were then analyzed with an image processing algorithm for extracting the melt pool area (MPA) from the process emission, as a key indicator for the process stability.

The algorithm consisted of three parts. Firstly, the NIR image was binarized applying static thresholding method, which converts the image into a matrix with elements equal to either 1 (white pixel) or 0 (black pixel) depending on whether the pixel's original value of grey level is higher/equal or lower than a threshold constant C . This procedure is expressed with the following equation:

$$p_{f,r,c}^T = \begin{cases} 1, & p_{f,r,c} \geq C \\ 0, & p_{f,r,c} < C \end{cases} \quad (5)$$

where $p_{f,r,c}$ is the gray level of the pixel in row r and column c of the frame f , and $p_{f,r,c}^T$ is the binary value of $p_{f,r,c}$ according to the threshold constant C . The threshold constant C was evaluated by matching the area computed from the NIR images with the area measured from externally illuminated images [14].

The second part of the algorithm consisted of removing the ejected particles and spatters from the NIR image, such that the algorithm recognizes and extracts only the melt pool.

Finally, the MPA of the frame f (MPA_f) was computed as the sum of all the white pixels found within the boundaries of the extracted melt pool blob:

$$MPA_f [mm^2] = r^2 \cdot \sum_{r=1}^m \sum_{c=1}^n p_{f,r,c}^T \quad (6)$$

where r is the spatial resolution.

Fig. 2 illustrates the algorithm procedure, initializing with the raw image, followed by thresholding, spatter elimination, and finally melt pool area extraction.

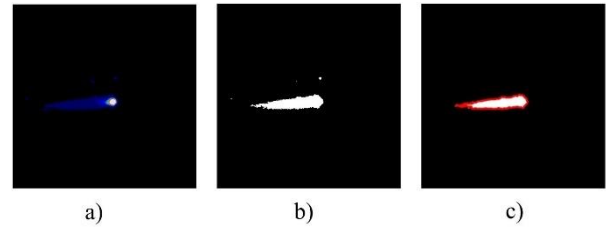


Fig. 2 Image analysis sequence: (a) raw image frame acquired during experimentation shown in false colors of intensity, (b) binarized image, (c) image after spatter removal and melt pool extraction. Each image shows an observation field of 4.3×4.3 mm².

4. DEVELOPMENT OF THE MODEL FOR ENERGY INPUT ADAPTATION

4.1. Experiment design

To develop the process model that estimates the nominal duty cycle (δ) per scan vector corresponding to the part geometry, an equilateral triangle with a side equal to 5 mm is chosen as a printing geometry since it provides continuous change of scan vector length. Each triangle specimen was printed with a constant duty cycle and consisted of 30 layers scanned with the same scanning direction and pattern. Each triangle is scanned starting from the longest scan vector and then continuing to the shortest one at the edge of the shape. The effect of the amount of energy density on the melt pool is investigated by varying the duty cycles from 0.3 to 1, where duty cycle equals to 1 corresponds to CW laser scanning mode. Each condition was replicated twice. The fixed and varied process parameters employed in the experiment are listed in Table 2. The fixed process parameters are confirmed through preliminary experiments to successfully fabricate a bulky part obtaining high density when the laser is scanning in CW mode.

To find the nominal melt pool area which indicates stable melting process, a square geometry with 5 mm side was scanned in CW mode, with process parameters which were preliminary proven to produce a high-density solid part with $\rho > 99.5\%$. A total of 30 layers were printed. Melt pool videos with the coaxial camera setup were acquired throughout the experiments.

Table 2 Fixed and varied scanning parameters employed during the experiment

Fixed parameters	
Layer thickness, z [μm]	50
Hatch distance, h [μm]	70
Scan speed, v [mm/s]	400
Peak power, P_{peak} [W]	200
Pulse repetition rate, PRR [kHz]	3
Scan direction [$^\circ$]	0
Scan strategy	Meander
Varied parameters	
Duty cycle, δ	0.3 – 1.0
Scan vector length, l_{sv} [mm]	0.05 – 5.0

4.2. Process modelling

Analyzing the melt pool images of the square sample, the nominal melt pool area indicating stable melting conditions was estimated as 0.46 mm^2 .

The process emission videos from the scanning process of the triangle samples showed that the melt pool is highly affected by the change of the average laser power and scan vector length. The average MPA per scan vector length (l_{sv}) and duty cycle (δ) is shown in Fig. 3. A decreasing trend of the melt pool area can be observed as the duty cycle decreases, while an increasing trend as the scan vector length decreases. This implies that scanning the sharp regions with high energy input results in MPA enlargement due to the lower time for heat dissipation, thus creating a defective region where swelling is observed. Considering the nominal melt pool area, the conditions causing overheating phenomenon can be observed when the MPA is larger than 0.46 mm^2 , and the conditions of undermelting when MPA is lower than 0.46 mm^2 . Therefore, it can be concluded that scanning with duty cycle lower than 0.7 always results in insufficient melting even in the small scan vector lengths. Furthermore, it is observed that employing the CW regime on the longer scan vector lengths ($\geq 4 \text{ mm}$) results in stable melting conditions and nominal MPA. Lastly, it is concluded that nominal MPA can be achieved throughout the whole processed geometry if the duty cycle is adapted per scan vector length.

A regression model was sought on the measured MPA using the two input variables (l_{sv} and δ). The following empirical model with $R_{adj}^2 = 98.61\%$ was fitted:

$$\ln(MPA) = -3.0153 + 3.843 \cdot \delta - 0.2241 \cdot l_{sv} - 0.86 \cdot \delta^2 + 0.00912 \cdot l_{sv}^2 \quad (7)$$

The P-value of the variables and their interaction showed

high statistical significance in describing the MPA (p-values were < 0.05), while the normality and homogeneity of the residuals were verified.

Knowing the nominal MPA, the duty cycle can be easily adapted as function of the scan vector length in order to deliver the optimal amount of energy input and to avoid defect generation in the fabricated part.

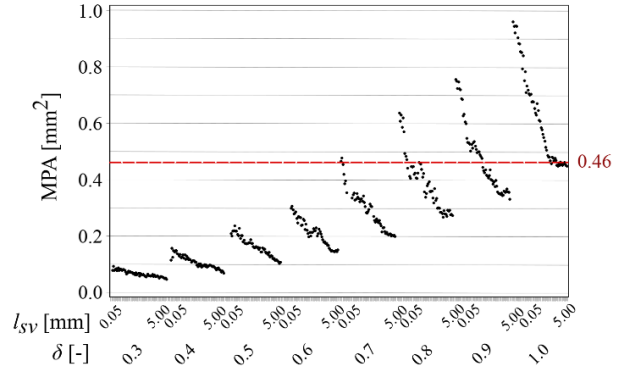


Fig. 3 Average MPA per scan vector length (l_{sv}) and duty cycle (δ) in the triangle specimens

Using the regression model, the energy density required to maintain the same MPA with varying scan vector could be calculated. The duty cycle relates to the laser energy density with the relation explained in Chapter 2. Fig. 4 presents the modeled duty cycle and the nominal density of the laser energy input per scan vector length, demonstrating the estimated amount of linear energy density decrease as the scan vector length reduces. The direct linear relationship found was used to modify the energy density by allocating the correct duty cycle as a function of the assigned vector length. Since the vectors are positioned prior to the process initiation, the process parameters could be changed offline similar to a feed forward control scheme.

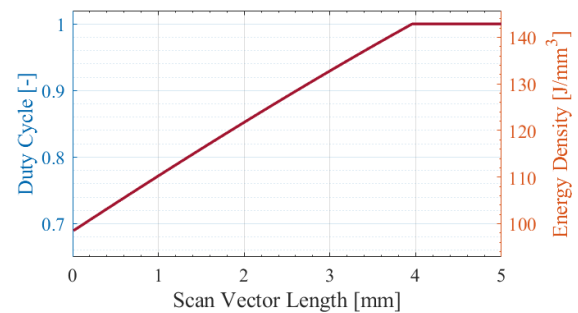


Fig. 4 Optimized duty cycle to achieve nominal MPA per scan vector length and the corresponding adapted laser energy density

5. MODEL VALIDATION

5.1. Experiment design

To validate the proposed model for energy input adaptation, experiments were carried out on a 4-point star and the already defined triangle, both containing sharp regions where swelling may occur due to extensive energy

input. Fig. 5 illustrates schematic of the geometry of the specimens as well as the scanning direction. Specimens without any parameter adaptation, thus scanned entirely in CW mode, were also produced for comparison, whereas the fixed parameters in all validation experiments were equivalent to the ones listed in Table 2. Each print consisted of 30 layers.

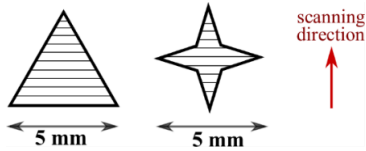


Fig. 5 Model validation geometries and scanning direction

In the specimens fabricated with adapted energy input, each scan vector was scanned with optimized duty cycle for attaining stable MPA.

To inspect the geometrical accuracy of the produced specimens, focus variation microscopy (Alicona Infinite Focus) was used for a three-dimensional reconstruction of the sample surfaces. Images were acquired using 5X magnification with estimated vertical and lateral resolutions of 1.1 μm and 7.83 μm , respectively. Mean square error of the surface geometry was calculated from the reconstructions.

5.2. Results

The three-dimensional reconstruction of the upper surface of the produced specimens is reported in Fig. 6 and Fig. 7, where the surface comparison of the parts produced with constant and with adapted energy input is visualized. In both parts scanned with CW regime, severe swelling is observed at the sharp regions where an excess of heat accumulation exhibits melt pool area enlargement resulting with faulty part. The mean square error of the surface geometry was lowered from 8.75 to 1.17 mm^2 for the triangle shape, and from 6.42 to 1.15 mm^2 for the 4-point star shape.

The specimens' macrographs are shown in Fig. 8 demonstrating the geometrical defect in the sharp region when employing constant duty cycle for scanning the hole part. Adapting the duty cycle depending on the part geometry proved to considerably improve the melting conditions and avoid the swelling occurrence due to overheating in short scan vectors in both geometries.

6. CONCLUSION

The present work demonstrates that adapting the laser energy input by modulating the laser power as a function of the part geometry, can produce stable melting process and avoid the generation of the swelling defect in critical sharp regions of the part. For assessing the melting conditions, a coaxial camera limited to the NIR process emission was employed. An image analysis algorithm for extracting the melt pool and calculating its area was developed.

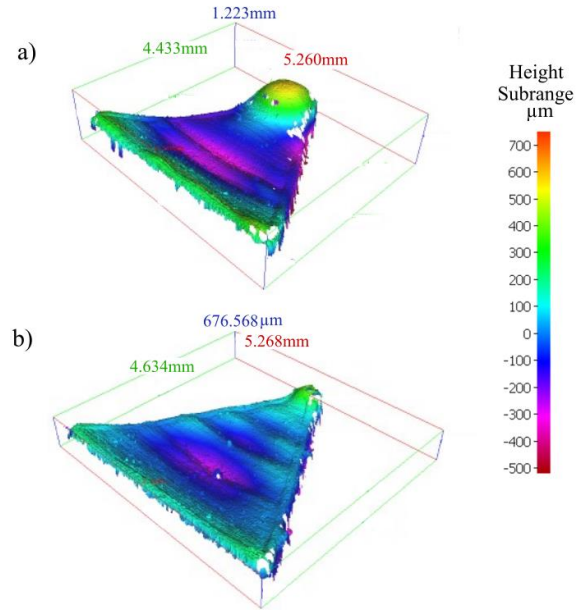


Fig. 6 3D reconstructions of the produced triangle specimens (a) without ($MSE = 8.75 \text{ mm}^2$) and (b) with the adapted energy input ($MSE = 1.17 \text{ mm}^2$).

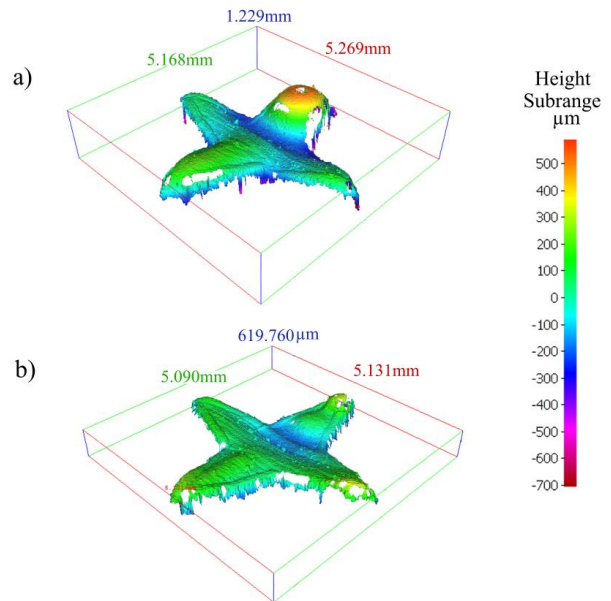


Fig. 7 3D reconstructions of the produced 4-point star specimens (a) without ($MSE = 6.42 \text{ mm}^2$) and (b) with the adapted energy input ($MSE = 1.15 \text{ mm}^2$).

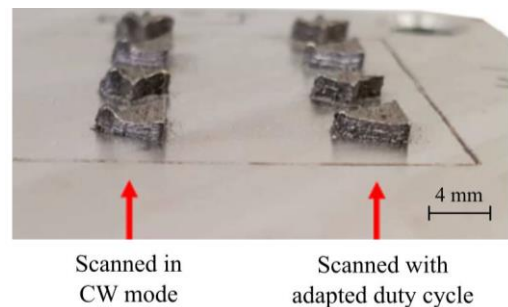


Fig. 8 Comparison of the produced specimens scanned with and without adapting the energy input

Experimental campaign showed that the melt pool is highly affected by the energy density input and the scan vector length. To assess the energy input, the duty cycle was selected as a variable process parameter modifying the delivered laser power, since it does not affect the process productivity. It was proven that when high laser energy was delivered in an acute corner constructed of small scan vector lengths, overheating occurred due to excessive heat accumulation resulting with enlargement of melt pool area, and thus surface swelling of the final part. Therefore, an empirical model was developed which estimates the nominal duty cycle to achieve stable melt pool depending on the single vector length, hence the part geometry. The model was validated on two geometries with critical edges. This work develops an empirical model that gives the correct amount of energy input. The model was validated on SLM prototype. The results showed that adapting the energy input improves geometrical deviations and avoids overheating phenomena in corner regions consisting of short scan vectors. The presented work does not for the microstructural defects. The developed empirical model has been also used to develop a layer-wise feedback control strategy on critical shapes [15] and overhanging structures [16].

ACKNOWLEDGEMENTS

The authors would like to thank IPG Italy and Optoprim for their technical support. The Italian Ministry of Education, University and Research is acknowledged for the support provided through the Project "Department of Excellence LIS4.0 - Lightweight and Smart Structures for Industry 4.0".

REFERENCES

- [1] C. Dordlofva, A. Lindwall, P. Törlind, Opportunities and challenges for additive manufacturing in space applications, *Proc. Nord. Nord.* 2016. 1 (2016).
- [2] J. V. Gordon, S.P. Narra, R.W. Cunningham, H. Liu, H. Chen, R.M. Suter, J.L. Beuth, A.D. Rollett, Defect structure process maps for laser powder bed fusion additive manufacturing, *Addit. Manuf.* 36 (2020) 101552. doi:10.1016/j.addma.2020.101552.
- [3] A. Charles, A. Elkaseer, L. Thijs, S.G. Scholz, Dimensional errors due to overhanging features in laser powder bed fusion parts made of Ti-6Al-4V, *Appl. Sci.* 10 (2020). doi:10.3390/app10072416.
- [4] E. Malekipour, H. El-Mounayri, Common defects and contributing parameters in powder bed fusion AM process and their classification for online monitoring and control: a review, *Int. J. Adv. Manuf. Technol.* 95 (2018) 527–550. doi:10.1007/s00170-017-1172-6.
- [5] J. zur Jacobsmühlen, S. Kleszczynski, G. Witt, D. Merhof, Detection of elevated regions in surface images from laser beam melting processes, in: *IECON 2015 - 41st Annu. Conf. IEEE Ind. Electron. Soc.*, 2015: pp. 1270–1275. doi:10.1109/IECON.2015.7392275.
- [6] I. Baturynska, O. Semeniuta, K. Martinsen, Optimization of Process Parameters for Powder Bed Fusion Additive Manufacturing by Combination of Machine Learning and Finite Element Method: A Conceptual Framework, *Procedia CIRP.* 67 (2018) 227–232. doi:10.1016/j.procir.2017.12.204.
- [7] M. Grasso, B.M. Colosimo, Process defects and *in situ* monitoring methods in metal powder bed fusion: a review, *Meas. Sci. Technol.* 28 (2017) 044005. doi:10.1088/1361-6501/aa5c4f.
- [8] L. Scime, J. Beuth, Using machine learning to identify in-situ melt pool signatures indicative of flaw formation in a laser powder bed fusion additive manufacturing process, *Addit. Manuf.* 25 (2019) 151–165. doi:10.1016/j.addma.2018.11.010.
- [9] J. Fox, F. Lopez, B. Lane, H. Yeung, S. Grantham, On the requirements for model-based thermal control of melt pool geometry in laser powder bed fusion additive manufacturing, *Mater. Sci. Technol. Conf. Exhib.* 2016, MS T 2016. 1 (2016) 133–140.
- [10] A.G. Demir, L. Mazzoleni, L. Caprio, M. Pacher, B. Previtali, Complementary use of pulsed and continuous wave emission modes to stabilize melt pool geometry in laser powder bed fusion, *Opt. Laser Technol.* 113 (2019) 15–26. doi:10.1016/j.optlastec.2018.12.005.
- [11] L. Caprio, A.G. Demir, B. Previtali, Comparative study between CW and PW emissions in selective laser melting, *J. Laser Appl.* 30 (2018) 032305. doi:10.2351/1.5040631.
- [12] L. Caprio, A.G. Demir, B. Previtali, Influence of pulsed and continuous wave emission on melting efficiency in selective laser melting, *J. Mater. Process. Technol.* 266 (2019). doi:10.1016/j.jmatprotec.2018.11.019.
- [13] B.M. Colosimo, E. Grossi, F. Caltanissetta, M. Grasso, Penelope: A Novel Prototype for In Situ Defect Removal in LPBF, *Jom.* 72 (2020) 1332–1339. doi:10.1007/s11837-019-03964-0.
- [14] M. Pacher, L. Mazzoleni, L. Caprio, A.G. Demir, B. Previtali, Estimation of melt pool size by complementary use of external illumination and process emission in coaxial monitoring of selective laser melting, *J. Laser Appl.* 31 (2019) 022305. doi:10.2351/1.5096117.
- [15] E. Vasileska, A.G. Demir, B.M. Colosimo, B. Previtali, Layer-wise control of selective laser melting by means of inline melt pool area measurements, *J. Laser Appl.* 32 (2020) 022057. doi:10.2351/7.0000108.

- [16] E. Vasileska, A.G. Demir, B.M. Colosimo, B. Previtali (in press), A novel paradigm for feedback control in LPBF: layer-wise correction for overhang structures, *Advances in Manufacturing*

NOTE

This paper is based on the paper presented at 14th International scientific conference MMA 2021 - FLEXIBLE TECHNOLOGIES Novi Sad, Serbia, September 23-25, 2021.